Stabilizing effect of optimally amplified streaks in parallel wakes

Gerardo Del Guercio[1,2], **Carlo Cossu**[1,†] **and Gregory Pujals**[2]

[1]CNRS – Institut de Mécanique des Fluides de Toulouse (IMFT), Allée du Professeur Camille Soula, F-31400 Toulouse, France

[2]PSA Peugeot Citroën, Centre Technique de Velizy, 2 Route de Gisy, 78943 Vélizy-Villacoublay CEDEX, France

We show that optimal perturbations artificially forced in parallel wakes can be used to completely suppress the absolute instability and to reduce the maximum temporal growth rate of the inflectional instability. To this end we compute optimal transient energy growths of stable streamwise uniform perturbations supported by a parallel wake for a set of Reynolds numbers and spanwise wavenumbers. The maximum growth rates are shown to be proportional to the square of the Reynolds number and to increase with spanwise wavelengths with sinuous perturbations slightly more amplified than varicose ones. Optimal initial conditions consist of streamwise vortices and the optimally amplified perturbations are streamwise streaks. Families of nonlinear streaky wakes are then computed by direct numerical simulation using optimal initial vortices of increasing amplitude as initial conditions. The stabilizing effect of nonlinear streaks on temporal and spatiotemporal growth rates is then determined by analysing the linear impulse response supported by the maximum amplitude streaky wakes profiles. This analysis reveals that at $Re = 50$, streaks of spanwise amplitude $A_s \approx 8\,\%U_\infty$ can completely suppress the absolute instability, converting it into a convective instability. The sensitivity of the absolute and maximum temporal growth rates to streak amplitudes is found to be quadratic, as has been recently predicted. As the sensitivity to two-dimensional (2D, spanwise uniform) perturbations is linear, three-dimensional (3D) perturbations become more effective than the 2D ones only at finite amplitudes. Concerning the investigated cases, 3D perturbations become more effective than the 2D ones for streak amplitudes $A_s \gtrsim 3\,\%U_\infty$ in reducing the maximum temporal amplification and $A_s \gtrsim 12\,\%U_\infty$ in reducing the absolute growth rate. However, due to the large optimal energy growths they experience, 3D optimal perturbations are found to be much more efficient than 2D perturbations in terms of initial perturbation amplitudes. Despite their lower maximum transient amplification, varicose streaks are found to be always more effective than sinuous ones in stabilizing the wakes, in accordance with previous findings.

Key words: absolute/convective instability, flow control, wakes/jets

† Email address for correspondence: carlo.cossu@imft.fr

1. Introduction

Vortex shedding in the wake of bluff bodies is a robust feature associated with undesirable unsteady loads and mean drag increase on the body. An important, enduring research effort aims at understanding the mechanisms by which the shedding self-sustains and how it could be attenuated or even suppressed. In the circular cylinder wake, the canonical flow used to test theories and control concepts, the shedding sets in at a critical Reynolds number (≈ 47) via a global instability. Self-sustained oscillations associated with global instability are supported by a finite region of local absolute instability near the body (see e.g. Chomaz, Huerre & Redekopp 1988; Huerre & Monkewitz 1990).

Different techniques have been proposed to suppress vortex shedding in two-dimensional wakes, among which an effective one is based on three-dimensional (3D) wake perturbations. Indeed, it has long been known that wrapping a helical cable around a cylinder (e.g. Zdravkovich 1981) or designing spanwise periodic trailing or leading edges of blunt bodies (starting with Tanner 1972, and followed by many others) can attenuate two-dimensional (2D) vortex shedding with a beneficial effect on mean drag and unsteady force peak fluctuations. We refer the reader to the review by Choi, Jeon & Kim (2008) for a clear discussion of these previous results and the associated references.

At low Reynolds numbers, 3D forcing can lead to the complete suppression of vortex shedding when spanwise wavelengths of the 3D perturbations are in the range of ≈ 1–6 diameters. In addition, 3D perturbations are found to require smaller perturbation amplitudes than spanwise uniform (2D) perturbations (Kim & Choi 2005). The nature and characteristics of the observed stabilizing effects have been mainly interpreted in terms of vorticity dynamics. Hwang, Kim & Choi (2013) (but see also Choi *et al.* 2008) have put forward an appealing explanation based on linear stability analysis. These authors convincingly show that spanwise modulations of parallel wake profiles lead to an attenuation of the absolute instability growth rate in a range of perturbation wavelengths than is in accordance with experimental and direct numerical simulation (DNS) findings. They also show that varicose perturbations are more effective than sinuous ones, in accordance with previous results of Kim *et al.* (2004), Kim & Choi (2005) and Park *et al.* (2006), and that for the amplitudes they consider, the absolute instability is far more sensitive to 2D than to 3D perturbations. However, from their study, it is not clear whether absolute instability can be completely suppressed and what is the effect of wake modulations on the maximum temporal growth rate of the instability, which affects the mode amplification in the convective region. Furthermore, in this previous analysis, a shape assumption is made on the 3D basic flow modification that neglects the nonlinear deformations appearing at moderate perturbation amplitudes.

A related problem, with a similar mathematical structure but quite different physical mechanisms involved, is that of stabilization of 2D boundary layers. In particular, Cossu & Brandt (2002, 2004) found that optimal 3D spanwise modulations (streamwise streaks) of the 2D Blasius boundary layer developing on a flat plate have a stabilizing effect on the 2D Tollmien–Schlichting instability, which develops above the critical Reynolds number. The optimal 3D perturbations used to control the boundary layer are those leading to the maximum energy growth in the linear approximation. Optimal spanwise periodic counter-rotating streamwise vortices are used to induce the transient growth of spanwise periodic streamwise streaks associated with spanwise modulations of the streamwise velocity profile. The optimal energy growth in this process is of $O(Re^2)$ (see e.g. Gustavsson 1991). The linearly

optimal vortices were then used, with finite amplitude, as input in fully nonlinear Navier–Stokes simulations to compute nonlinearly saturated streaks. The 2D (spanwise averaged) modification of the boundary layer profile induced by the 3D streaks plays a crucial role in the stabilization (Cossu & Brandt 2002). This 2D modification is not captured by simply adding linear streaks to the boundary layer profile. It was also found that a key stabilizing role is played by the work of Reynolds shear stresses against the spanwise basic flow shear Cossu & Brandt (2004). The stabilizing action of streaks on TS waves and the effective delay of transition to turbulence using this technique was later confirmed experimentally (Fransson *et al.* 2005, 2006).

Inspired by the type of analysis developed for boundary layers, one may therefore wonder if similar conclusions can be reached in plane 2D wakes. Some natural questions that arise are as follows. Can large transient energy growths of spanwise periodic perturbations be supported by 2D wakes? If yes, how does the maximum energy growth scale with the Reynolds number? Do nonlinearly saturated streamwise streaks have a stabilizing effect on the wake inflectional instability? If yes, what level of growth rate reductions can be attained? Do nonlinearly saturated optimal streamwise streaks have a stabilizing effect on the wake absolute instability? How would these effects relate to those described by Hwang *et al.* (2013)? Is it possible to completely suppress the absolute instability? Does the nonlinear spanwise mean (2D) flow distortion play an important role in the stabilizing mechanism? How is the stabilizing effect related to the work of Reynolds stresses? The scope of the present investigation is to try to answer these questions.

The analysis will be developed on parallel wake profiles proposed by Monkewitz (1988), which have been used as a laboratory for stability analyses of plane wakes in a number of previous studies, such as those of Delbende & Chomaz (1998), Hwang & Choi (2006) and Hwang *et al.* (2013). The advantage of this approach is that the results are genuinely related to the wake structure, and not to the specific generating body's surface shape and physics.

After a brief description of the problem setup, given in § 2, the optimal energy growths, inputs and outputs supported by the considered wake profiles are computed and discussed in § 3. The temporal and spatiotemporal stability of nonlinear streak profiles issued by linear optimal initial conditions is analysed in § 4. A summary and discussion of the main results are reported in § 5. Details of the method used in the computation of optimal energy growths, in the direct numerical simulations and in the extraction of the temporal and spatiotemporal stability results from the numerical simulation of the impulse response are given in the Appendix.

2. Mathematical model

In the following, essentially two kinds of basic flows will be considered. The first type is the usual (spanwise uniform i.e. 2D) parallel wake $\boldsymbol{U}_M = \{U_M(y), 0, 0\}$, where the streamwise velocity profile $U_M(y)$ is the one proposed by Monkewitz (1988):

$$U_M(y) = 1 + \Lambda \left[\frac{2}{1 + \sinh^{2N}(y \sinh^{-1} 1)} - 1 \right], \quad (2.1)$$

with $\Lambda = (U_c^* - U_\infty^*)/(U_\infty^* + U_c^*)$, U_c^* the centreline and U_∞^* the free stream velocity (dimensional variables are starred). The velocity profile U_M is made dimensionless with respect to the reference velocity $U_{ref}^* = (U_c^* + U_\infty^*)/2$. The spatial coordinates are made dimensionless with respect to the reference length δ^*, which is the distance from the centreline to the point where the 2D wake velocity is equal to U_{ref}^*. In the

following we consider the value $\Lambda = -1$, corresponding to a zero centreline velocity, which has been used by Delbende & Chomaz (1998) and Hwang *et al.* (2013), for example, and the shear concentration parameter value $N = 1$, which corresponds to the same shear profile as the Bickley jet. The $U_M(y)$ profile obtained with these parameters is shown in figure 3(*a*).

In addition to the standard 2D wakes, the stability of spanwise modulated 3D 'streaky wakes' $\boldsymbol{U} = \{U(y, z), 0, 0\}$ will be considered in the following (where we let x denote the streamwise direction, y the transverse and z the spanwise one). For both types of wake profiles, the evolution of perturbations $\boldsymbol{u}', p'$ to the basic flow wake $\boldsymbol{U}, P$ is ruled by the Navier–Stokes equations, written in perturbation form as

$$\nabla \cdot \boldsymbol{u}' = 0, \tag{2.2}$$

$$\frac{\partial \boldsymbol{u}'}{\partial t} + (\nabla \boldsymbol{U})\boldsymbol{u}' + (\nabla \boldsymbol{u}')\boldsymbol{U} + (\nabla \boldsymbol{u}')\boldsymbol{u}' = -\nabla p' + \frac{1}{Re}\nabla^2 \boldsymbol{u}'. \tag{2.3}$$

The flow is assumed incompressible and the fluid viscous with kinematic viscosity ν. The Reynolds number $Re = U_{ref}^* \delta^* / \nu$ is based on the characteristic velocity and length scale of the basic flow which are used to make dimensionless velocities and lengths. In the linearized stability framework the term $(\nabla \boldsymbol{u}')\boldsymbol{u}'$ is neglected.

3. Optimal perturbations of 2D wakes

The first step of our analysis consists in finding the optimal initial perturbations leading to the maximum amplification of the kinetic energy of the response at time t. For parallel basic flows the optimal growths of Fourier modes $\widehat{\boldsymbol{u}}(\alpha, y, \beta, t)\mathrm{e}^{\mathrm{i}(\alpha x + \beta z)}$ of streamwise and spanwise wavenumbers α and β can be considered separately. The optimal temporal energy amplification G is defined, in the usual way, as the ratio of the kinetic energy density associated with $\widehat{\boldsymbol{u}}$ at time t to the kinetic energy of the initial condition $\widehat{\boldsymbol{u}}_0$ optimized over non-zero $\widehat{\boldsymbol{u}}_0$, $G(\alpha, \beta, t) = \sup_{\widehat{\boldsymbol{u}}_0} \|\widehat{\boldsymbol{u}}\|^2 / \|\widehat{\boldsymbol{u}}_0\|^2$, where $\|\widehat{\boldsymbol{u}}\|^2 = (1/\mathscr{V}_{ref}) \int_{\mathscr{V}} |\widehat{\boldsymbol{u}}|^2 \, d\mathscr{V}$ and $\mathscr{V}_{ref} = 2\delta L_x L_z$ in the present case. Two-dimensional parallel wakes, like the one defined in (2.1), are unstable to inflectional instabilities if Re is not too small. For the values $Re \gtrsim 25$ considered in this study, an unstable region exists in the (α, β) plane centred around the 2D ($\beta = 0$) unstable waveband $0 < \alpha \lesssim 1.75$. In this study we are not interested in the optimal amplification of unstable perturbations but in their stabilization by optimally amplified stable disturbances. We will therefore consider the optimal growth of streamwise uniform ($\alpha = 0$) perturbations, both because they mimic the perturbations that would be spatially forced by steady passive devices and because they are linearly stable.

As the U_M profile is symmetric with respect to $y = 0$, perturbations to this profile are separated into varicose perturbations, for which $\widehat{u}(-y) = \widehat{u}(y)$, $\widehat{v}(-y) = -\widehat{v}(y)$, $\widehat{w}(-y) = \widehat{w}(y)$, and sinuous perturbations that have opposite symmetry properties. Standard methods, described in §A.1, have been used to compute $G(t)$ for both varicose and sinuous perturbations for $Re = 25, 50$ and 100 and for spanwise wavenumbers β ranging from 0.1 to 2 with $\alpha = 0$. For all these parameters the computed $G(t)$ curves typically have a single maximum $G_{max}(\alpha = 0, \beta, Re) = \sup_t G(t, \alpha = 0, \beta, Re)$, attained at t_{max}, and tend to zero for large times. The maximum optimal growths G_{max} computed for sinuous perturbations are reported in figure 1(*a*) as a function of β for the selected Reynolds numbers. From this figure it is seen how G_{max} increases with Re. From the analysis of Gustavsson (1991) it is expected that for streamwise uniform perturbations G_{max} and t_{max} are proportional to Re^2 and Re respectively. This is indeed verified for both G_{max} (see figure 1*b*) and t_{max} (not shown).
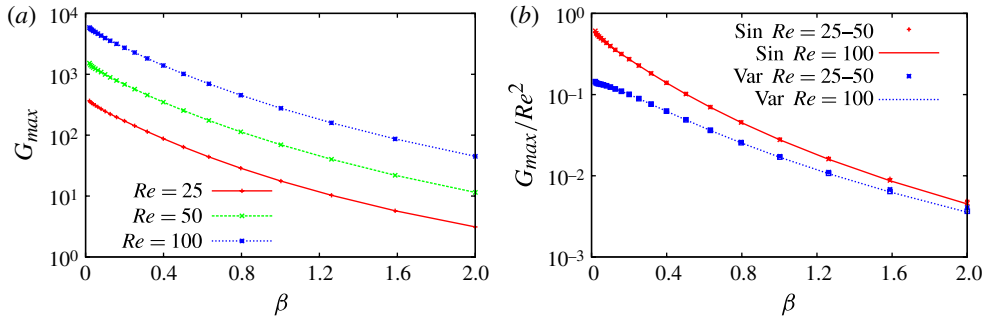
FIGURE 1. (Colour online) (*a*) Dependence of the maximum growth rate G_{max} of streamwise uniform ($\alpha = 0$) sinuous perturbations on the spanwise wavenumber β for three selected Reynolds numbers Re. (*b*) Rescaled maximum growth rate G_{max}/Re^2 dependence on β for sinuous (solid line, red) and varicose (dashed line, blue) perturbations. The lines correspond to the rescaled $Re = 100$ data, while the $Re = 25$ and $Re = 50$ rescaled data are shown as points. It can be seen how, when rescaled, data obtained at different Re collapse onto the same curve.

The maximum growths G_{max} and the associated t_{max} are also seen to increase with the perturbation spanwise wavelength $\lambda_z = 2\pi/\beta$, at least in the λ_z range examined. Varicose perturbations follow the same trend as sinuous ones, with the same Re scaling and a similar increase with λ_z of G_{max}, but are slightly less amplified than sinuous perturbations, as shown in figure 1(*b*).

Similar to what has been found in wall-bounded shear flows, optimal initial conditions correspond to spanwise periodic streamwise vortices while the most amplified perturbations correspond to spanwise periodic streamwise streaks. Optimal perturbations computed for $Re = 50$ and $\beta = 1$ are reported in figure 2. In the case of varicose perturbations (figure 2*a*), there are two antisymmetric rows of vortices on each side of the wake symmetry axis inducing symmetric streaks, while in the case of sinuous perturbations (figure 2*b*), a single row of vortices centred on the wake symmetry axis induces antisymmetric streaks. When the spanwise wavenumber β is decreased (the spanwise wavelength $\lambda_z = 2\pi/\beta$ is increased), the size of optimal perturbations increases in both the spanwise and the normal direction y, as shown in figure 3. The velocity of optimal varicose initial vortices is, non-negligible up to $y \approx \lambda_z$, which highlights the difficulty of forcing optimal perturbations with low values of β in practical applications such as those based on the body's leading and trailing edge deformation (Bearman & Owen 1998; Darekar & Sherwin 2001, e.g.) or on blowing and suction (Kim & Choi 2005).

4. Influence of streaks on wake stability

4.1. *Basic flow streaky wakes*

Nonlinear streaky wakes are computed following the same rationale used in previous studies of the stability of streaks in wall-bounded flows, such as those of Reddy *et al.* (1998), Andersson *et al.* (2001), Brandt *et al.* (2003), Cossu & Brandt (2004) and Park, Hwang & Cossu (2011). Optimal linear perturbations (streamwise vortices) with finite initial amplitude A_0 are used as initial condition $\boldsymbol{U}_{I0}(y, z) = \boldsymbol{U}_M(y) + A_0 \boldsymbol{u}_I^{(opt)}(y, z)$, where $\|\boldsymbol{u}_I^{(opt)}\| = 1$. The nonlinear Navier–Stokes equations are then numerically integrated for the selected initial conditions (see § A.2 for numerical details), providing
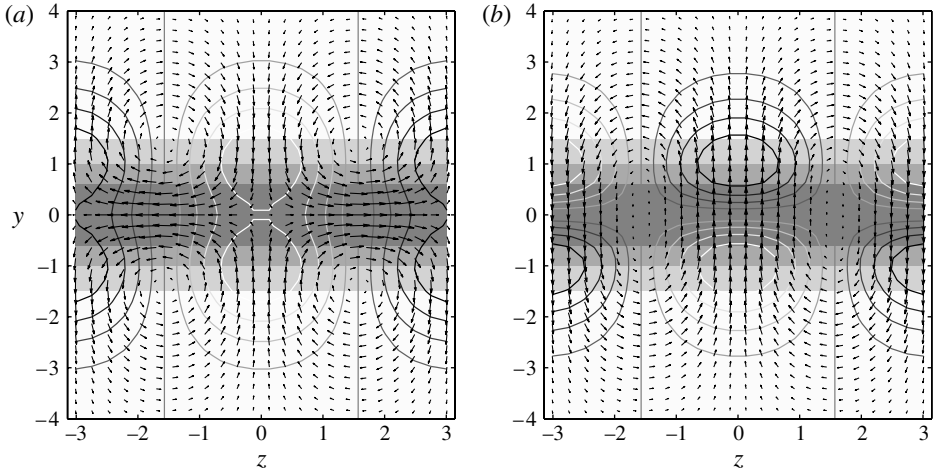
FIGURE 2. Cross-stream view of the v'–w' components of optimal initial vortices (arrows) and of the u' component of the corresponding maximally amplified streak (contour lines) for $Re = 50$ and $\beta = 1, \alpha = 0$. Optimal varicose perturbations are reported in (a), while sinuous ones are reported in (b). The 2D basic flow wake streamwise velocity is shown in grey-scale, with white corresponding to the free stream velocity and dark grey to zero (wake centreline).
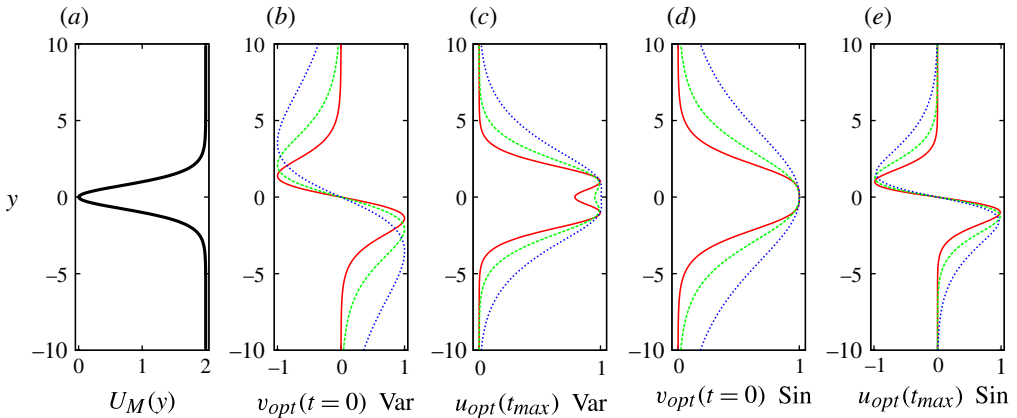

FIGURE 3. (Colour online) Normalized amplitude of the $\widehat{v}(y)$ component of the optimal initial ($t = 0$) vortices (b,d) and the $\widehat{u}(y)$ component of the corresponding optimally amplified ($t = t_{max}$) streaks (c,e), corresponding to the varicose (b,c) and sinuous (d,e) perturbations, for $\beta = 1$. i.e. $\lambda_z = 6.28$ (solid, red). $\beta = 0.5$. i.e. $\lambda_z = 12.56$ (dashed, green). and $\beta = 0.25$. i.e. $\lambda_z = 25.13$ (dotted, blue). The 2D wake basic flow profile $U_M(y)$ is also reported in (a) for comparison.

a family of basic flows $\boldsymbol{U}_I(y, z, t, A_0)$, parametrized by A_0 for the Reynolds number considered. The amplitude of the streaks is measured, extending the definition proposed by Andersson et al. (2001):

$$A_s(t, A_0) = \frac{1}{2} \frac{\max_{y,z}(U_I(y, z, t, A_0) - U_M(y)) - \min_{y,z}(U_I(y, z, t, A_0) - U_M(y))}{\max_y U_M(y) - \min_y U_M(y)}. \quad (4.1)$$
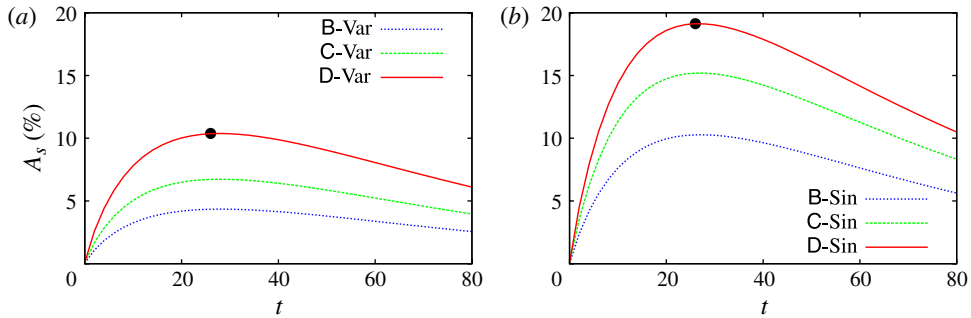
FIGURE 4. (Colour online) Temporal evolution of nonlinear streak amplitude $A_s(t)$ for selected initial amplitudes A_0 of the initial optimal perturbations and for varicose (*a*) and sinuous (*b*) perturbations. For all cases, $Re = 50$ and $\beta = 1$. See table 1 for the legend of cases and the associated initial amplitudes A_0.

Case	A	B-Var	C-Var	D-Var	B-Sin	C-Sin	D-Sin
A_0	0	1.25×10^{-2}	1.94×10^{-2}	3.00×10^{-2}	2.00×10^{-2}	2.93×10^{-2}	3.66×10^{-2}
$A_{s,max}$	0	4.35%	6.73%	10.38%	10.27%	15.02%	18.80%

TABLE 1. The nonlinear streaky wakes considered. A_0 is the finite initial amplitude given to the linear optimal perturbations. $A_{s,max}$ is the maximum streak amplitude reached in the nonlinear numerical simulation. Case A corresponds to the reference two-dimensional wake profile $U_M(y)$. Cases B, C and D are obtained by increasing A_0.

In figure 4 we display the temporal evolution of the amplitudes of nonlinear streaks for $Re = 50$ and $\beta = 1$, for varicose and sinuous perturbations of selected amplitudes. As reported in table 1, case A corresponds to the reference two-dimensional wake profile $U_M(y)$ (no streaks), while cases B, C and D are obtained by increasing the initial optimal perturbation amplitude A_0.

In the following we will analyse the local spatiotemporal instability properties of the streaky wake profiles 'frozen' at the time of maximum streak amplitude, following the approach used by Reddy *et al.* (1998), Andersson *et al.* (2001), Brandt *et al.* (2003), Cossu & Brandt (2004) and Park *et al.* (2011), among others. The local analysis is justified by the fact that streaks decay slowly (for example, the varicose D streak changes its amplitude by $\approx 4\%$ in $\Delta t \approx 50$) when compared to the fast growth of unstable perturbations (typical maximum growth rates are of the order of $1/4$, and therefore during $\Delta t \approx 50$ they would have been amplified by a factor of $e^{50/4} \approx 270\,000$). The streaky basic flows corresponding to the varicose and sinuous case D are reported in figure 5.

4.2. *Stability analysis based on linear impulse response*

The linear stability properties of streaky wake profiles, including the convective or absolute nature of any instability, are revealed by the analysis of the linear impulse response (Green's function) that they support. The basic flow is linearly stable if the amplitude of impulse response tends to zero as $t \to \infty$ and unstable otherwise. In the unstable case, the instability is absolute if the impulse response amplitude grows in the position of the initial pulse, while it is convective if it grows while being advected
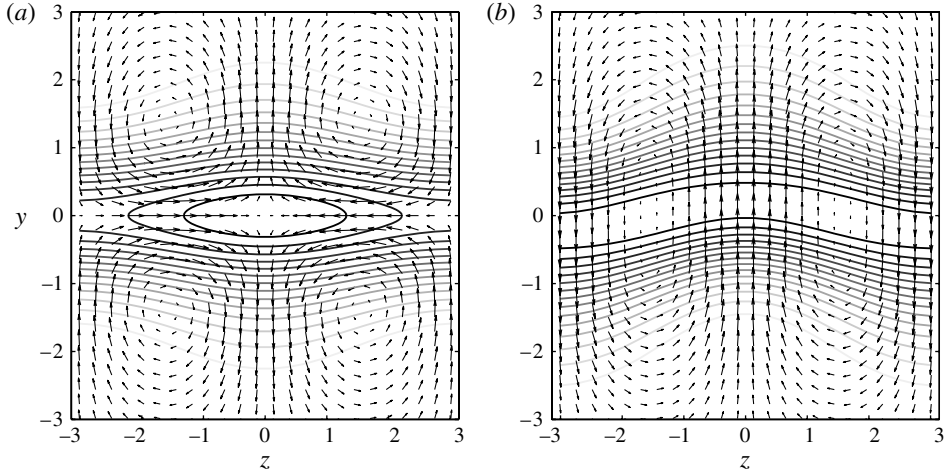
FIGURE 5. Cross-stream view of case D varicose (*a*) and sinuous (*b*) nonlinear streaky wake basic flows. Contour lines, iso-levels of the total streamwise velocity $U_I(y, z)$ extracted at the time of maximum amplitude (black circles in figure 4); arrows, v–w components of optimal initial vortices given as initial condition at $t = 0$.

by the flow but eventually tends to zero in the position of the initial pulse (Huerre & Monkewitz 1990).

The linear impulse response is computed by direct numerical simulation of the Navier–Stokes equations linearized near the frozen streaky basic flow profiles $U_I(y, z, t, A_0)$ described in § 4.1. To mimic forcing by a delta function in time and space, the initial condition is defined in terms of a 2D stream function as

$$\psi'(x, y, z) = A_{II} e^{-((x-x_0)^2/2\sigma_x^2)-((y-y_0)^2/2\sigma_y^2)-((z-z_0)^2/2\sigma_z^2)}, \qquad (4.2)$$

which is the three-dimensional extension of the initial condition used by Delbende & Chomaz (1998) for the same type of analysis of 2D wakes. The corresponding perturbation velocity components are given by $(u', v', w') = (\partial\psi/\partial y, -\partial\psi/\partial x, 0)$ and the amplitude A_{II} is set sufficiently small to avoid overflows during the linear simulation. The parameters $\sigma_x = 0.83$, $\sigma_y = 0.83$ and $\sigma_z = 0.30$ have been chosen small enough to reproduce a localized impulse within the limits of a good resolution. The impulse is centred at $x_0 = 62$, $y_0 = 1$, $z_0 = \pi/4$, ensuring that no particular symmetry is preserved by the initial condition.

According to standard Floquet theory (see e.g. Nayfeh & Mook 1979), normal modes of the spanwise periodic basic flow of spanwise wavelength λ_z may be sought in the form

$$q(x, y, z, t) = \tilde{q}(y, z)e^{i(\alpha x+\gamma\beta z-\omega t)}, \qquad (4.3)$$

where q is the generic flow variable. $\gamma \in [0, 1/2]$ is the detuning parameter and ω is the complex frequency. Hwang *et al.* (2013) found absolute instabilities in spanwise modulated wakes only for fundamental ($\gamma = 0$) and subharmonic ($\gamma = 1/2$) modes. Fundamental modes have the same spanwise periodicity λ_z as the basic flow, while subharmonic modes have periodicity $2\lambda_z$. Both types of mode will be considered together by performing numerical simulations in a spanwise periodic domain of length $L_z = 2\lambda_z$. In this framework, the spanwise z-variable is an eigenfunction direction just
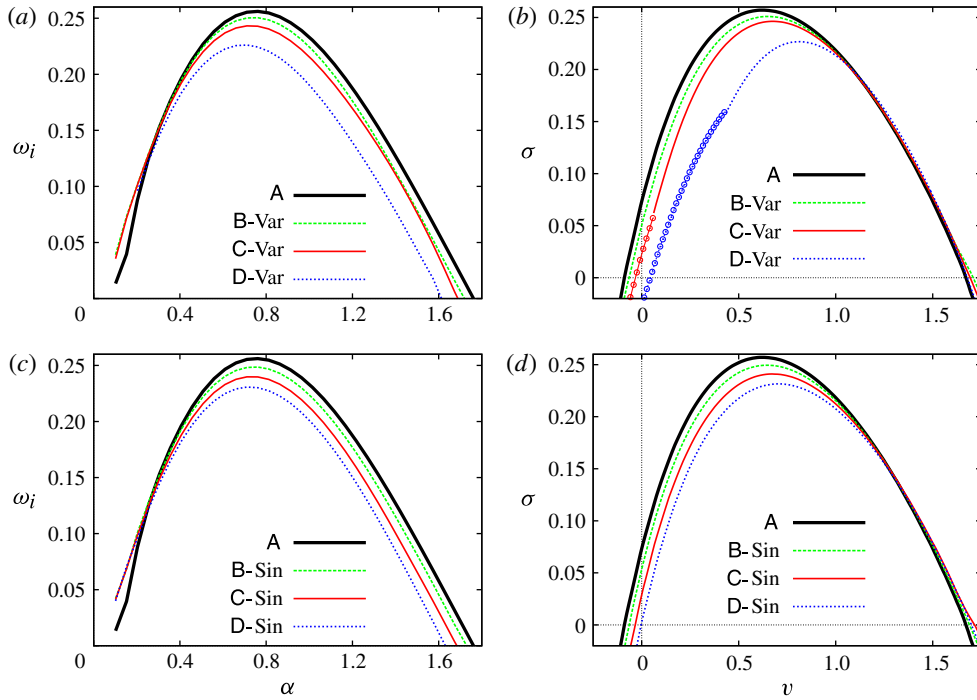
FIGURE 6. (Colour online) Stabilizing effect of varicose (*a,b*) and sinuous (*c,d*) streaks on temporal (*a,c*) and spatiotemporal (*b,d*) growth rates of linear perturbations. Case A corresponds to the 2D reference wake while cases B, C and D correspond to increasing streak amplitudes. The basic flow is absolutely unstable if $\sigma(v = 0) > 0$. The presence of symbols on parts of the stability curves denotes the range where subharmonic modes are dominating.

as the transverse y variable. Note that only one initial pulse is enforced at $t = 0$ in the given 'doubled' domain. The growth rates of fundamental and subharmonic, symmetric and antisymmetric modes can be separated using spanwise Fourier transforms. In particular, fundamental modes have harmonics with wavenumbers $\beta_n^{(F)} = n\beta$, while for subharmonic modes $\beta_n^{(S)} = (n + 1/2)\beta$ with $n = 1, 2, \ldots$ and where β is the spanwise wavenumber of the basic flow streaks (fundamental wavenumber). Further details are given in § A.3.

The temporal growth rate curves $\omega_i(\alpha)$ are extracted from the numerically computed impulse response as described in § A.4 and are reported in figure 6. The 2D reference wake, case A, as is well known, is linearly unstable with a maximum growth rate $\omega_{i,max} = 0.256$. When streaks of increasing amplitude are forced, the maximum growth rate is reduced. The leading modes have the same symmetries in z as basic flow profiles (fundamental–symmetric in the terminology of § A.3), and varicose streaks are found to be more effective at stabilizing the temporal instability. For instance, $\omega_{i,max}$ is reduced by $\approx 12\%$ using varicose streaks with $A_s \approx 10\%$ (case D-Var) and by 10 % for sinuous streaks with $A_s \approx 18\%$ (case D-Sin).

The absolute or convective nature of the instability can be determined from the spatiotemporal growth rate $\sigma(v)$, which is the temporal growth rate observed by an observer travelling along the spatiotemporal ray $x/t = v$. For the considered wake profiles, which are unstable, $\sigma > 0$ in the range $v \in [v^-, v^+]$, where v^- and v^+

are respectively the trailing and leading edge velocities of the wave packet. In the present situation, therefore, the instability is absolute for $\sigma(v = 0) > 0$, i.e. if $v^- < 0$. The maximum value of σ corresponds to the maximum temporal growth rate $\omega_{i,max}$. The $\sigma(v)$ curves have been extracted from the numerically computed impulse responses following the standard procedure explained in § A.4, which has already been used by Delbende & Chomaz (1998) and Brandt *et al.* (2003) and Lombardi *et al.* (2011), among others; these are shown in figure 6. The 2D reference wake (case A) is absolutely unstable with an absolute growth rate $\sigma(v = 0) = 0.073$ and the wave-packet trailing-edge travelling upstream with velocity $v^- = -0.089$. The absolute growth rate is reduced when streaks of increasing amplitude are forced, and can become negative for sufficiently large streak amplitudes transforming the absolute instability into a convective instability. Varicose streaks are found to be more effective at stabilizing the absolute instability than sinuous streaks. The varicose streak D-Var with $A_s \approx 10\%$ is already convectively unstable, while amplitudes above $A_s \approx 18\%$ (case D-Sin) are necessary for sinuous streaks to drive the instability from absolute to convective. For sinuous streaks, the leading modes in the $\sigma(v)$ curves are fundamental–symmetric (the same symmetries as the basic flow streaks in the spanwise direction). For varicose streaks, fundamental–symmetric modes are the leading ones, except for large-amplitude streaks at sufficiently small values of v, where subharmonic–antisymmetric modes are dominant and therefore control the quenching of the absolute instability.

4.3. *Sensitivity to basic flow modifications and cost of the stabilization*

By an asymptotic (small-amplitude) sensitivity analysis, Hwang & Choi (2006) have shown that the absolute growth rate variation depends linearly on the amplitude of spanwise uniform (2D) perturbations of the basic flow. Hwang *et al.* (2013) show that the sensitivity to spanwise sinusoidal (3D) basic flow perturbations depends quadratically on their amplitudes. To verify whether these predictions extend to the nonlinear streaks considered and to maximum temporal growth rate sensitivity, we report in figure 7 the dependence of the maximum growth rate $\omega_{i,max}$ and of the wave-packet trailing edge velocity v^- on the streak amplitude A_s. We consider v^- and not $\sigma(v = 0)$ as a measure of the absolute or convective nature of the instability because the numerical method used (impulse response analysis) does not provide well-converged results for negative growth rates. We also consider the effect on the stability of a 2D (spanwise uniform) perturbation with a profile $u_{2D}(y)$ equal to the high-speed varicose streak profile $\hat{u}(y)$. The amplitude A_s of this 2D basic flow modification is defined by (4.1), but removing the 1/2 factor that accounted for the presence of high- and low-speed streaks. From figure 7 it is seen that $\omega_{i,max}$ and v^- do indeed depend quadratically on A_s for streaky basic flow modifications, but linearly for a 2D basic flow modification. The conclusions of the sensitivity analysis of Hwang *et al.* (2013) are therefore confirmed by the present results, despite the fact that in our computations, for increasing A_s nonlinear streaks change not only their amplitude but also, slightly, their shape. Considering the stabilization of the maximum temporal growth rate, the quadratic sensitivity of the streaks to A_s, even if it gives a weaker effect than 2D basic flow modifications at very small streak amplitudes, can provide a larger effect at larger A_s. This is not the case for the quenching of absolute instability, where 2D basic flow modifications are able to drive v^- to positive values for lower A_s values than 3D basic flow modifications, as already remarked by Hwang *et al.* (2013). However, as the streaks have been forced using linearly optimal initial conditions, it is interesting to analyse the dependence of the stabilizing actions not only on the basic flow distortion
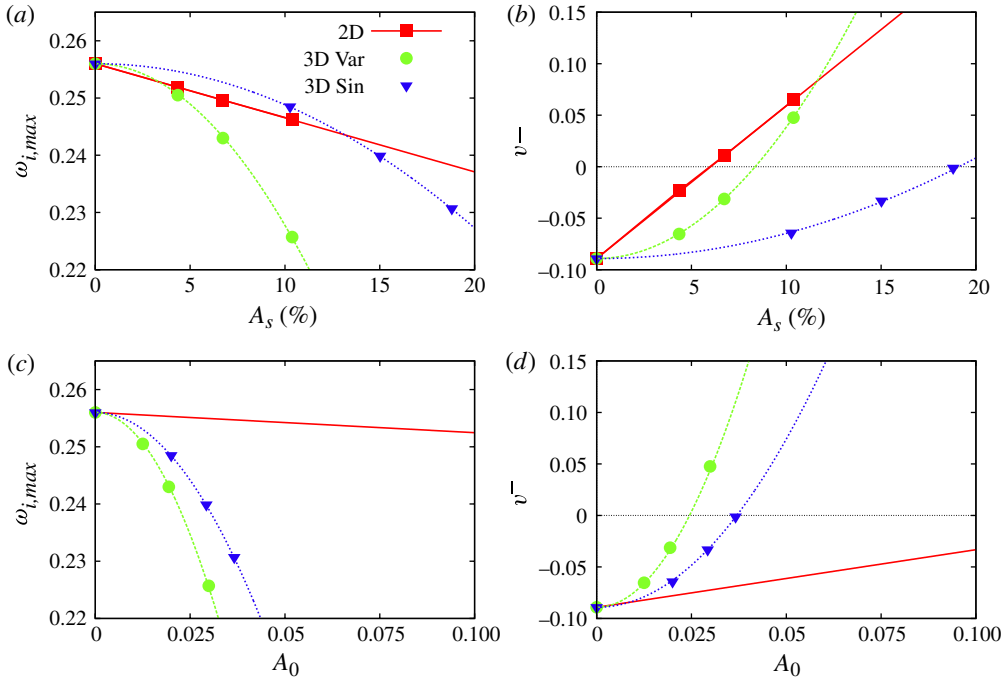
FIGURE 7. (Colour online) Dependence of the maximum growth rate $\omega_{i,max}$ (a,c) and the wave-packet trailing edge velocity v^- (b,d) on the streak amplitude A_s (a,b) and the initial disturbance amplitude A_0 (c,d). Zero amplitudes correspond to the 2D wake reference case. A (2D) spanwise uniform perturbation has been also considered for comparison. Symbols denote data points, while lines are linear and quadratic best fits to the data points.

amplitude A_s but on the amplitude A_0 of the initial perturbation based on energy density:

$$A_0^2 = \frac{1}{2\delta L_x L_z} \int_0^{L_x} \int_{-\infty}^{\infty} \int_0^{L_z} \boldsymbol{u}'_0 \cdot \boldsymbol{u}'_0 \, \mathrm{d}x \, \mathrm{d}y \, \mathrm{d}z. \tag{4.4}$$

This dependence is also reported in figure 7, where, again quadratic and linear sensitivities of $\omega_{i,max}$ and v^- on A_0 are found for 3D and 2D basic flow perturbations respectively. When the amplitude of initial conditions is considered, however, optimal 3D perturbations are shown to be more effective than 2D perturbations at stabilizing the flow. This is not surprising because, in a first approximation, a factor of $\sqrt{2G_{max}}$ is gained through the lift-up effect when forcing optimal 3D streaks using optimal initial vortices instead of enforcing the 2D profile with the same streak shape. For the presently considered case, for instance, the absolute–convective instability transition is enforced with optimal 3D streaks with values of A_0 more than six times smaller than those necessary when using 2D basic flow modifications (one hundred times smaller in terms of kinetic energy). Note also that the lift-up amplitude gain increases like Re (like Re^2 in terms of energy), and therefore the cost of forcing 3D perturbations of given amplitude decreases when the Reynolds number is increased. These results suggest that the key ingredient of the success of wake control strategies based on 3D flow modifications mainly relies on the large energy gains associated with the lift-up effect.

Case	A	D-Var	$\overline{\mathsf{D}}$-Var	$\widetilde{\mathsf{D}}$-Var	$\widetilde{\mathsf{D}}_{lin}$-Var
$\omega_{i,max}$	0.2560	0.2257	0.2495	0.2305	0.2262
v^-	$-0.089\,050$	0.047\,561	-0.0052	0.022\,891	0.017\,337

TABLE 2. Comparison of maximum growth rate $\omega_{i,max}$ and of the wave-packet trailing edge velocity v^- computed for the unperturbed wake (case A, profile $U_M(y)$), the genuine varicose streak D (profile $U_M(y) + \Delta U(y,z)$) and the 'synthetic' streaks $\overline{\mathsf{D}}$-Var (with profile $U_M(y) + \overline{\Delta U}(y)$), $\widetilde{\mathsf{D}}$-Var (with profile $U_M(y) + \widetilde{\Delta U}(y,z)$) and $\overline{\mathsf{D}}_{lin}$-Var (with profile $U_M(y) + \widetilde{\Delta U}_{lin}(y,z)$).

5. Analysis of the stabilizing mechanism

5.1. *Role of streaks' 2D mean flow distortion in the stabilizing mechanism*

In §4.2 it has been shown that the forcing of streaks has a stabilizing effect on $\omega_{i,max}$ and v^-. One important question concerns the stabilizing mechanism. In the case of the stabilization of boundary layer instability it was found that a crucial role was played by the (nonlinear) spanwise mean flow distortion. Following Cossu & Brandt (2002), we therefore separate the wake distortion $\Delta U(y,z) = U(y,z) - U_M(y)$ induced by the streaks into the spanwise averaged part $\overline{\Delta U}(y)$ and the spanwise varying part $\widetilde{\Delta U}(y,z) = \Delta U(y,z) - \overline{\Delta U}(y)$. Nonlinear effects are necessary to generate $\overline{\Delta U}(y)$. To evaluate the respective effects of the spanwise periodic streak component $\widetilde{\Delta U}$ and of the basic flow spanwise mean distortion $\overline{\Delta U}$, we have repeated the impulse response analysis on the artificial basic flows $\widetilde{\mathsf{D}}$-Var and $\overline{\mathsf{D}}$-Var obtained by taking into account only the spanwise varying or the spanwise uniform part of the basic flow distortion, i.e. $U_{\widetilde{D}} = U_M + \widetilde{\Delta U}$ and $U_{\overline{D}} = U_M + \overline{\Delta U}$. The values of $\omega_{i,max}$ and of v^- pertaining to these artificial basic flows are compared to those obtained for the genuine streaky wake D-Var in table 2. From this table it is seen that, in contrast to what is found in boundary layers, the streaks' stabilizing action is not to be attributed to the 2D mean flow distortion $\overline{\Delta U}(y)$ but to its 3D spanwise varying part $\widetilde{\Delta U}$, which is, for example, able to quench the absolute instability on its own. To understand whether streak deformations due to nonlinearities are relevant in the stabilization mechanism, the additional synthetic streaky wake $\widetilde{\mathsf{D}}_{lin}$-Var has been considered. Its velocity profile $U_M(y) + \widetilde{\Delta U}_{lin}(y,z)$ is obtained by adding the linear optimal streak profile to the reference 2D wake with the same amplitude as streak D. The results show that the stabilization induced by this linear streak is comparable to that induced by both $\widetilde{\Delta U}$ and the full streak ΔU, which are all able to quench the absolute instability.

5.2. *Analysis of kinetic energy production and dissipation terms*

Further insight into the mechanism by which the streaks stabilize the wake inflectional instability can be gained by the analysis of the different terms contributing to temporal growth of total perturbation kinetic energy, which is the well-known Reynolds–Orr equation (see e.g. Schmid & Henningson 2001):

$$\frac{1}{2}\frac{d}{dt}\int_{\mathscr{V}} \boldsymbol{u}' \cdot \boldsymbol{u}' \, d\mathscr{V} = -\int_{\mathscr{V}} \boldsymbol{u}' \otimes \boldsymbol{u}' : \boldsymbol{\nabla U} \, d\mathscr{V} - \frac{1}{Re}\int_{\mathscr{V}} \boldsymbol{\nabla u}' : \boldsymbol{\nabla u}' \, d\mathscr{V}. \qquad (5.1)$$

This equation states that the rate of change of perturbation kinetic energy is given by the sum of a production term, given by the work of Reynolds stresses against the

Case	$\omega_{i,max}$	$\widehat{P}_y/2\widehat{K}$	$\widehat{P}_z/2\widehat{K}$	$-\widehat{D}/2\widehat{K}$
A	0.256 00	0.298 20	0.000 00	−0.043 20
B-Var	0.249 26	0.295 58	−0.001 31	−0.045 01
C-Var	0.243 07	0.293 34	−0.004 26	−0.046 01
D-Var	0.225 34	0.292 84	−0.008 62	−0.058 88

TABLE 3. Maximum temporal growth rates and normalized kinetic energy production and dissipation components pertaining to the varicose streaky wakes.

basic flow shear, and a dissipation term, which is always negative. Cossu & Brandt (2004) have shown that for perturbations in the form of normal modes $\widehat{\boldsymbol{u}}(y, z)\mathrm{e}^{\mathrm{i}(\alpha x - \omega t)}$, the Reynolds–Orr equation reduces to the following decomposition for the temporal growth rate:

$$\omega_i = \frac{\widehat{P}_y}{2\widehat{K}} + \frac{\widehat{P}_z}{2\widehat{K}} - \frac{\widehat{D}}{2\widehat{K}}, \tag{5.2}$$

with the definitions

$$\widehat{K} = \frac{1}{\lambda_z} \int_0^{\lambda_z} \int_{-\infty}^{\infty} (\widehat{u}\widehat{u}^* + \widehat{v}\widehat{v}^* + \widehat{w}\widehat{w}^*) \,\mathrm{d}y \,\mathrm{d}z, \tag{5.3}$$

$$\widehat{P}_y = \frac{1}{\lambda_z} \int_0^{\lambda_z} \int_{-\infty}^{\infty} -(\widehat{u}\widehat{v}^* + \widehat{u}^*\widehat{v}) \frac{\partial U}{\partial y} \,\mathrm{d}y \,\mathrm{d}z, \tag{5.4}$$

$$\widehat{P}_z = \frac{1}{\lambda_z} \int_0^{\lambda_z} \int_{-\infty}^{\infty} -(\widehat{u}\widehat{w}^* + \widehat{u}^*\widehat{w}) \frac{\partial U}{\partial z} \,\mathrm{d}y \,\mathrm{d}z, \tag{5.5}$$

$$\widehat{D} = \frac{1}{\lambda_z} \int_0^{\lambda_z} \int_{-\infty}^{\infty} 2(\widehat{\xi}\widehat{\xi}^* + \widehat{\eta}\widehat{\eta}^* + \widehat{\zeta}\widehat{\zeta}^*) \,\mathrm{d}y \,\mathrm{d}z, \tag{5.6}$$

where $\widehat{\boldsymbol{u}} = (\widehat{u}, \widehat{v}, \widehat{w})$ are the three velocity components of the normal mode and $(\widehat{\xi}, \widehat{\eta}, \widehat{\zeta})$ the corresponding vorticity components. The different terms of (5.2) have been computed for the varicose streaky wakes considered in §4 and are reported in table 3 in correspondence to the most amplified streamwise wavenumber α_{max} for which the maximum growth rate $\omega_{i,max}$ is obtained. As it is well known, the instability of the 2D reference wake is explained by the large production term $\widehat{P}_y$, which exceeds the dissipation term $\widehat{D}$ when the Reynolds number is not exceedingly low. The forcing of streaks induces a stabilizing effect on all the components contributing to the growth rate. Not only is the $\widehat{P}_y$ production term reduced and the dissipation term increased, but the additional production term $\widehat{P}_z$ comes into play with a stabilizing effect. The stabilizing action on all the terms increases when the streak amplitude is increased and is of the same order of magnitude for all terms.

6. Summary of the main results and discussion
6.1. *Summary of main results*

Concerning optimal energy growth of stable perturbations supported by 2D parallel wakes, in the first part of the study we have shown the following.

(i) Parallel 2D wakes can sustain large transient growths of 3D streamwise uniform perturbations that are linearly stable. For instance, the maximum growth supported by perturbations of spanwise wavelength $\lambda_z = 2\pi$ ($\beta = 1$) is $G_{max} = 70$ at $Re = 50$.

(ii) The maximum energy growth is proportional to Re^2 in accordance with what is observed in other shear flows. Therefore, for instance, at $Re = 100$ the maximum energy growth of $\lambda_z = 2\pi$ perturbations is four times larger ($G_{max} = 280$) than at $Re = 50$.

(iii) Maximum energy growth also increases with spanwise perturbation wavelengths (i.e. for decreasing β), but in this case optimal perturbations correspond to structures of ever larger cross-stream extension that would probably be difficult to enforce in practical applications. This result is similar to what is observed, for example, in vortex columns in unbounded domains (Pradeep & Hussain 2006).

(iv) The most amplified perturbations are sinuous. Varicose perturbations are slightly less amplified (but by less than a factor of two). Optimal initial perturbations consist of streamwise vortices that induce the growth of streamwise streaks that modulate the wake's streamwise velocity in the spanwise direction. The cross-stream shape of the width of the wake is sinuous or varicose depending on the enforced perturbations.

In the second part of the study, we analysed the influence on stability of nonlinear streak modulations of the wake enforced by optimal initial streamwise vortices of increasing amplitude. The specific values $\beta = 1$, $Re = 50$ were considered. We have shown the following.

(i) Nonlinear streamwise streaks induced by optimal initial vortices reduce both the maximum temporal growth rate and the absolute growth rate of the inflectional instability.

(ii) Varicose streaks are more stabilizing than sinuous streaks of the same amplitude.

(iii) It is possible to suppress the absolute instability with small streak amplitudes ($A_s \approx 8\,\% U_\infty$).

(iv) The decrease of the maximum growth rate and of the absolute instability depends quadratically on the amplitude of streaks and on the amplitude of initial perturbations used to force them.

(v) When compared to 2D basic flow perturbations, whose stabilizing effect is linearly proportional to their amplitude, 3D varicose streak perturbations are more efficient in terms of amplitude A_s, when $A_s \gtrsim 3\,\% U_\infty$ with respect to maximum temporal amplification and $A_s \gtrsim 12\,\% U_\infty$ when absolute growth rates are considered. However, when the comparison is made in terms of the required initial perturbation amplitude A_0, optimal 3D perturbations are much more efficient than 2D perturbations (more than six times). This is due to the efficiency of the lift-up effect leading to large energy growths, with the efficiency increasing with Reynolds number. Varicose perturbations remain more efficient than sinuous ones even when their initial amplitude A_0 is considered, despite the fact that their optimal linear growth is lower.

(vi) Contrary to what is observed in the stabilization of boundary layers by streaks, the spanwise averaged nonlinear mean-flow distortion induced by nonlinear streaks does not play a crucial role in the stabilization. The spanwise oscillating part of the streaks plays the most important role, with optimal linear streak shapes as effective as nonlinear streak shape in the stabilization.

(vii) The decomposition of the maximum temporal growth rate into the different components due to energy production and dissipation shows that the streaks' stabilizing action acts on all these components by increasing the energy dissipation, reducing the 2D-type energy production and inducing a stabilizing (negative) energy production term related to the work of Reynolds stress against basic flow spanwise shear.

6.2. *Discussion*

As discussed in §1, the second part of the study is strongly related to a set of previous investigations on vortex shedding, quenching or weakening enforced via 3D basic flow modulations. The stabilizing effect we find is indeed in agreement with numerous previous studies showing that spanwise modulations of the bluff body shape or spanwise modulated blowing and suction can have a stabilizing effect on vortex shedding (see Choi *et al.* 2008). In particular, in a very recent investigation, Hwang *et al.* (2013) have shown that 3D spanwise modulations of the 2D wake streamwise velocity reduce the absolute growth rate of unstable perturbations supported by Monkewitz (1988) wake profiles. Our results confirm the findings of Hwang *et al.* (2013), and in particular the stabilizing effect on absolute instability, the fact that varicose perturbations are more effective than sinuous ones, and the quadratic sensitivity of the absolute growth rate to the amplitude of 3D basic flow modifications. However, we extend their investigation by showing that by using streaks of moderate but still not excessive amplitudes, absolute instability can be completely suppressed, and not only reduced. Also, more insight into the stabilizing mechanism has been given by its analysis in terms of spanwise mean and oscillating contributions to the stabilization and in terms of respective contributions of the work of Reynolds stresses and of the dissipation to the stabilizing mechanism. The main conclusion here is that the success of vortex shedding 3D basic flow modifications can be attributed both to the very efficient amplification of streamwise streaks that ultimately stabilize the flow and to the quadratic dependence of the stabilization on their amplitude. This quadratic dependence, which is a weak point at very low amplitudes, allows high sensitivity to 3D basic flow modifications at larger amplitudes, where practically relevant effects are attained.

Another relevant result that extends what was previously known is that not only absolute growth rates but also maximum temporal growth rates are reduced by enforcing optimal streaks. The growth rate reductions we have documented are moderate, but probably much larger reductions can be achieved by forcing streaks of only slightly larger amplitude, thanks to the quadratic sensitivity of the growth rate reductions on streak amplitudes (see figure 7). As both optimal perturbations, maximum energy growth supported by parallel 2D wakes and modal growth rates of parallel 3D wakes are unchanged by the addition of a uniform velocity, our results, except for the absolute instability analysis, directly extend to, say, jets with the same shear profile.

Only parallel wakes have been considered in the present investigation, both because the main interest is on local stability properties, and also for the sake of conciseness and clarity. It will nonetheless be important to complete the study by computing optimal perturbations in a non-parallel spatial stability setting, similar to what has been done for boundary layers by Andersson, Berggren & Henningson (1999), for example, and to assess the influence of those optimal perturbations on global stability. As unstable global modes in non-parallel wakes are sustained by a pocket of local absolute instability, it is expected that forcing streaks of sufficiently large amplitude

could stabilize the global instability. Such a stabilizing action is, however, not expected to apply to situations where the basic flow non-parallelism alters the nature of the global instability, such as in wakes developing behind rotating cylinders (Pralits, Giannetti & Brandt 2013). These issues are currently under close scrutiny. The present analysis is also currently being extended to the turbulent case where 3D mean flow modifications are also effective at attenuating von Kármán vortex shedding (e.g. Kim & Choi 2005), proceeding along the same lines as in wall-bounded shear flows (Cossu, Pujals & Depardon 2009; Pujals *et al.* 2009; Hwang & Cossu 2010; Pujals, Depardon & Cossu 2010).

Acknowledgements

Appendix. Methods

A.1. *Computation of optimal perturbations*

Optimal growths $G(t, \alpha, \beta)$ are computed along quite standard lines, described in Schmid & Henningson (2001), for example. The linearized Navier–Stokes equations are recast in terms of the cross-stream velocity and vorticity v–η. The system satisfied by Fourier modes, $\widehat{v}(y, t; \alpha, \beta)e^{i(\alpha x + \beta z)}$, $\widehat{\eta}(y, t; \alpha, \beta)e^{i(\alpha x + \beta z)}$, is the standard Orr–Sommerfeld–Squire system,

$$\nabla^2 \frac{\partial \widehat{v}}{\partial t} = \mathscr{L}_{\mathscr{OS}} \widehat{v}; \quad \frac{\partial \widehat{\eta}}{\partial t} = -i\beta \frac{dU}{dy} \widehat{v} + \mathscr{L}_{\mathscr{SQ}} \widehat{\eta}, \tag{A 1}$$

where the Orr–Sommerfeld and Squire operators are

$$\mathscr{L}_{\mathscr{OS}} = -i\alpha \left[U(\mathscr{D}^2 - k^2) - \frac{d^2 U}{dy^2} \right] + \frac{1}{Re}(\mathscr{D}^2 - k^2)^2, \tag{A 2}$$

$$\mathscr{L}_{\mathscr{SQ}} = -i\alpha U + \frac{1}{Re}(\mathscr{D}^2 - k^2), \tag{A 3}$$

and where $\mathscr{D}$ denotes d/dy and $k^2 = \alpha^2 + \beta^2$. The system is discretized on a grid of N_y points uniformly distributed in $[-L_y/2, L_y/2]$. Differentiation matrices based on second-order accurate finite differences have been used to discretize the Orr–Sommerfeld–Squire system. Most of the results have been obtained with $N_y = 201$ and L_y, ranging from 20 to 120 for the perturbations with the smallest spanwise wavenumbers (largest spanwise wavelengths). The results do not change when N_y is doubled to 401 and when L_y is increased by half. We have also verified that the results do not change if differentiation matrices are based on Fourier series instead of finite differences, provided that L_y is large enough. The discretization has also been validated against temporal growth rates of Bickley jets available in the literature. Once the linear operator is discretized, standard methods and codes already used in previous investigations (e.g. Lauga & Cossu 2005; Cossu *et al.* 2009; Pujals *et al.* 2009) are used to compute the optimal growth and the associated optimal perturbations.

A.2. *Direct numerical simulations*

Numerical simulations of nonlinear and linearized Navier–Stokes equations have been performed using the *OpenFOAM* open-source DNS code (see http://www.openfoam.org). We have modified the code to allow for the solution of the Navier–Stokes equation in perturbation form and in order to add a set of additional output data.

The flow is solved inside the domain $[0, L_x] \times [-L_y/2, L_y/2] \times [0, L_z]$, which is discretized using a grid with N_x and N_z equally spaced points in the streamwise and spanwise directions respectively. N_y points are used in the y direction using a stretching that allows us to increase point density in the region where the basic flow shear is not negligible. Typically, results have been obtained using $L_x = 124$, $L_y/2 = 10$, $L_z = 2\pi$ and $N_x = 300$, $N_y = 160$, $N_z = 24$ with $\Delta x = 0.4$, $\Delta z = 0.26$ and a minimum of $\Delta y = 0.01$ on the symmetry axis and a maximum of $\Delta y = 0.1$ near the free stream boundary. Periodic boundary conditions have been used in the streamwise and spanwise directions and zero normal gradients of velocity and pressure have been enforced at the free stream boundaries ($|y| = L_y/2$). An increase of $L_y/2$ from 10 to 15 or an increase of the number of points from $N_y = 160$ to $N_y = 320$ did not affect the energy density more than 2 %. Also, the combined results of the DNS and the stability analysis algorithms described below have been checked against existing results both for the temporal stability analysis (temporal growth rates of the Bickley jet) and the temporal and spatiotemporal growth rates of Monkewitz profiles.

A.3. *Fundamental and subharmonic, symmetric and antisymmetric modes*

As mentioned in § 4.2, the numerical simulations of the linear impulse response are performed in a spanwise periodic domain of length twice that of the basic flow streaks $L_z = 2\lambda_z$ where $\lambda_z = 2\pi/\beta$. The impulse response can be decomposed into the contributions of fundamental and subharmonic modes, which can be further decomposed into symmetric and antisymmetric. The fundamental modes with an even symmetry (the same as that of the basic flow streaks) are of the form with $\beta_k^F = k\beta$, where β is the wavenumber of the basic flow streaks:

$$\widehat{u}(y, z) = \sum_{k=1}^{\infty} \tilde{u}_k(y) \cos \beta_k^F z, \quad \widehat{v}(y, z) = \sum_{k=1}^{\infty} \tilde{v}_k(y) \cos \beta_k^F z, \quad \widehat{w}(y, z) = \sum_{k=1}^{\infty} \tilde{w}_k(y) \sin \beta_k^F z.$$

(A 4)

Fundamental modes with the opposite symmetry admit the expansions

$$\widehat{u}(y, z) = \sum_{k=1}^{\infty} \tilde{u}_k(y) \sin \beta_k^F z, \quad \widehat{v}(y, z) = \sum_{k=1}^{\infty} \tilde{v}_k(y) \sin \beta_k^F z, \quad \widehat{w}(y, z) = \sum_{k=1}^{\infty} \tilde{w}_k(y) \cos \beta_k^F z.$$

(A 5)

For subharmonic modes the spanwise periodicity of the disturbances is twice that of the basic flow, and therefore we define $\beta_k^S = [(k + 1)/2]\beta$. Subharmonic–symmetric modes are expanded as

$$\widehat{u}(y, z) = \sum_{k=1}^{\infty} \tilde{u}_k(y) \cos \beta_k^S z, \quad \widehat{v}(y, z) = \sum_{k=1}^{\infty} \tilde{v}_k(y) \cos \beta_k^S z, \quad \widehat{w}(y, z) = \sum_{k=1}^{\infty} \tilde{w}_k(y) \sin \beta_k^S z,$$

(A 6)

while subharmonic–antisymmetric modes admit the expansions

$$\widehat{u}(y, z) = \sum_{k=1}^{\infty} \tilde{u}_k(y) \sin \beta_k^S z, \quad \widehat{v}(y, z) = \sum_{k=1}^{\infty} \tilde{v}_k(y) \sin \beta_k^S z, \quad \widehat{w}(y, z) = \sum_{k=1}^{\infty} \tilde{w}_k(y) \cos \beta_k^S z.$$

(A 7)

Given a perturbation velocity field, obtained from linearized DNS, for example, the respective contributions of the fundamental and subharmonic, symmetric and

antisymmetric modes to the total field can be retrieved by a straightforward partitioning of the spanwise discrete Fourier transform of the velocity field into odd/even harmonic real/imaginary parts.

A.4. *Temporal and spatiotemporal stability analysis from the impulse response*

The techniques used to retrieve the temporal and spatiotemporal stability properties of parallel basic flow profile $U(y, z)$ from the numerically computed impulse response closely follow those used by Brandt *et al.* (2003), which are the three-dimensional extension of those developed by Delbende & Chomaz (1998) and Delbende, Chomaz & Huerre (1998) for two-dimensional wakes.

Consider the generic perturbation variable $q(x, y, z, t)$, already separated into its fundamental and subharmonic, symmetric and antisymmetric parts as described in § A.3. Concerning the temporal stability analysis, in order to determine the dependence of the temporal growth rate ω_i on the (real) streamwise wavenumber α, the amplitude spectrum of $q(x, y, z, t)$ is defined as

$$
\widetilde{Q}(\alpha, t) = \left(\int_{-L_y/2}^{L_y/2} \int_0^{L_z} |\tilde{q}(\alpha, y, z, t)|^2 \, dy \, dz \right)^{1/2},
\tag{A 8}
$$

where $\tilde{q}(\alpha, y, z, t)$ is the Fourier transform of the variable q in the streamwise direction. The asymptotic exponential regime is attained for large times, where the leading temporal mode emerges with growth rate (imaginary part of ω) well approximated by

$$
\omega_i(\alpha) \sim \frac{\partial}{\partial t} \ln \widetilde{Q}(\alpha, t), \quad t \to \infty,
\tag{A 9}
$$

which can be numerically computed by the finite difference approximation

$$
\omega_i(\alpha) \approx \frac{\ln[\widetilde{Q}(\alpha, t_2)/\widetilde{Q}(\alpha, t1)]}{t_2 - t_1}.
\tag{A 10}
$$

The selected times t_1 and t_2 in the above approximation need to be sufficiently large to ensure the extinction of transients. The values used for the presented results have been selected by exploring different pairs t_1, t_2 until results have satisfactorily converged to less than 1 % relative error.

The spatiotemporal stability analysis considers the development of the impulse response wave packet along $x/t = v$ rays, which is equivalent to the investigation of modes of real group velocity v (see e.g. Huerre & Rossi 1998). The use of the Hilbert transform allows us to demodulate the wave packet and define its amplitude unambiguously with respect to spatial phase oscillations. To this end, the analytical complex field variable $q_H(x, y, z, t)$ associated with $q(x, y, z, t)$ through the x-convolution $*$ is defined as

$$
\bar{q}(x, y, z, t) = \left[\delta(x) + \frac{i}{\pi x} \right] * q(x, y, z, t).
\tag{A 11}
$$

In wavenumber space, (A 11) reduces to

$$
q_H(\alpha, y, z, t) = 2H(\alpha)\tilde{q}(\alpha, y, z, t),
\tag{A 12}
$$

where $H(\alpha)$ is the Heaviside unit-step function. The integration of the analytical field q_H in the cross-stream (y, z) plane then yields the amplitude Q defined by

$$Q(x, t) = \left(\int_{-L_y/2}^{L_y/2} \int_0^{L_z} |q_H(x, y, z, t)|^2 \, dy \, dz \right)^{1/2}. \quad (A\,13)$$

According to steepest-descent arguments (e.g. Bers 1983), the long-time behaviour of the wave packet along each spatiotemporal ray $x/t = v$ is

$$Q(x, t) \propto t^{-1/2} e^{i[\alpha(v)x - \omega(v)t]}, \quad t \to \infty, \quad (A\,14)$$

where $\alpha(v)$ and $\omega(v)$ represent the complex wavenumber and frequency travelling at the group velocity v. In (A 14), the real part of the exponential

$$\sigma(v) = \omega_i(v) - k_{x,i}(v)v \quad (A\,15)$$

denotes the temporal growth rate observed while travelling at the velocity v, and it can be evaluated for large t directly from the amplitude Q in (A 14) as

$$\sigma(v) \sim \frac{\partial}{\partial t} \ln[t^{1/2} Q(vt, t)], \quad (A\,16)$$

which can be approximated with

$$\sigma(v) \approx \frac{\ln[Q(vt_2, t_2)/Q(vt_1, t_1)]}{t_2 - t_1} + \frac{\ln(t_2/t_1)}{2(t_2 - t_1)}, \quad (A\,17)$$

to which apply the same considerations discussed for (A 10).

REFERENCES

ANDERSSON, P., BERGGREN, M. & HENNINGSON, D. 1999 Optimal disturbances and bypass transition in boundary layers. *Phys. Fluids* **11** (1), 134–150.

ANDERSSON, P., BRANDT, L., BOTTARO, A. & HENNINGSON, D. 2001 On the breakdown of boundary layer streaks. *J. Fluid Mech.* **428**, 29–60.

BEARMAN, P. W. & OWEN, J. C. 1998 Reduction of bluff-body drag and suppression of vortex shedding by the introduction of wavy separation lines. *J. Fluids Struct.* **12** (1), 123–130.

BERS, A. 1983 Space–time evolution of plasma instabilities: absolute and convective. In *Handbook of Plasma Physics,* vol. 1 (ed. M. N. Rosenbluth & R. Z. Sagdeev), pp. 451–517. North-Holland.

BRANDT, L., COSSU, C., CHOMAZ, J.-M., HUERRE, P. & HENNINGSON, D. S. 2003 On the convectively unstable nature of optimal streaks in boundary layers. *J. Fluid Mech.* **485**, 221–242.

CHOI, H., JEON, W. P. & KIM, J. 2008 Control of flow over a bluff body. *Annu. Rev. Fluid Mech.* **37**, 357–392.

CHOMAZ, J. M., HUERRE, P. & REDEKOPP, L. G. 1988 Bifurcations to local and global modes in spatially developing flows. *Phys. Rev. Lett.* **60**, 25–28.

COSSU, C. & BRANDT, L. 2002 Stabilization of Tollmien–Schlichting waves by finite amplitude optimal streaks in the Blasius boundary layer. *Phys. Fluids* **14**, L57–L60.

COSSU, C. & BRANDT, L. 2004 On Tollmien–Schlichting waves in streaky boundary layers. *Eur. J. Mech.* B **23**, 815–833.

COSSU, C., PUJALS, G. & DEPARDON, S. 2009 Optimal transient growth and very large-scale structures in turbulent boundary layers. *J. Fluid Mech.* **619**, 79–94.

DAREKAR, R. M. & SHERWIN, S. J. 2001 Flow past a square-section cylinder with a wavy stagnation face. *J. Fluid Mech.* **426** (1), 263–295.

DELBENDE, I. & CHOMAZ, J.-M. 1998 Nonlinear convective/absolute instabilities of parallel two-dimensional wakes. *Phys. Fluids* **10**, 2724–2736.

DELBENDE, I., CHOMAZ, J.-M. & HUERRE, P. 1998 Absolute and convective instabilities in the Batchelor vortex: a numerical study of the linear impulse response. *J. Fluid Mech.* **355**, 229–254.

FRANSSON, J., BRANDT, L., TALAMELLI, A. & COSSU, C. 2005 Experimental study of the stabilization of Tollmien–Schlichting waves by finite amplitude streaks. *Phys. Fluids* **17**, 054110.

FRANSSON, J., TALAMELLI, A., BRANDT, L. & COSSU, C. 2006 Delaying transition to turbulence by a passive mechanism. *Phys. Rev. Lett.* **96**, 064501.

GUSTAVSSON, L. H. 1991 Energy growth of three-dimensional disturbances in plane Poiseuille flow. *J. Fluid Mech.* **224**, 241–260.

HUERRE, P. & MONKEWITZ, P. A. 1990 Local and global instabilities in spatially developing flows. *Annu. Rev. Fluid Mech.* **22**, 473–537.

HUERRE, P. & ROSSI, M. 1998 Hydrodynamic instabilities in open flows. In *Hydrodynamic and Nonlinear Instabilities* (ed. C. Godrèche & P. Manneville), pp. 81–294. Cambridge University Press.

HWANG, Y. & CHOI, H. 2006 Control of absolute instability by basic-flow modification in a parallel wake at low Reynolds number. *J. Fluid Mech.* **560**, 465–475.

HWANG, Y. & COSSU, C. 2010 Amplification of coherent streaks in the turbulent Couette flow: an input–output analysis at low Reynolds number. *J. Fluid Mech.* **643**, 333–348.

HWANG, Y., KIM, J. & CHOI, H. 2013 Stabilization of absolute instability in spanwise wavy two-dimensional wakes. *J. Fluid Mech.* **727**, 346–378.

KIM, J. & CHOI, H. 2005 Distributed forcing of flow over a circular cylinder. *Phys. Fluids* **39**, 033103.

KIM, J., HAHN, S., KIM, J., LEE, D., CHOI, J., JEON, W. & CHOI, H. 2004 Active control of turbulent flow over a model vehicle for drag reduction. *J. Turbul.* **5** (19).

LAUGA, E. & COSSU, C. 2005 A note on the stability of slip channel flows. *Phys. Fluids* **17**, 088106.

LOMBARDI, M., CAULFIELD, C. P., COSSU, C., PESCI, A. I. & GOLDSTEIN, R. E. 2011 Growth and instability of a laminar plume in a strongly stratified environment. *J. Fluid Mech.* **671**, 184–206.

MONKEWITZ, P. A. 1988 The absolute and convective nature of instability in two-dimensional wakes at low Reynolds numbers. *Phys. Fluids* **31**, 999–1006.

NAYFEH, A. H. & MOOK, D. T. 1979 *Nonlinear Oscillations*. Wiley-Interscience.

PARK, J., HWANG, Y. & COSSU, C. 2011 On the stability of large-scale streaks in turbulent Couette and Poiseuille flows. *C. R. Méc.* **339**, 1–5.

PARK, H., LEE, D., JEON, W. P., HAHN, S., KIM, J. & CHOI, H. 2006 Drag reduction in flow over a two-dimensional bluff body with a blunt trailing edge using a new passive device. *J. Fluid Mech.* **563**, 389–414.

PRADEEP, D. S. & HUSSAIN, F. 2006 Transient growth of perturbations in a vortex column. *J. Fluid Mech.* **550**, 251–288.

PRALITS, J. O., GIANNETTI, F. & BRANDT, L. 2013 Three-dimensional instability of the flow around a rotating circular cylinder. *J. Fluid Mech.* **730**, 5–18.

PUJALS, G., DEPARDON, S. & COSSU, C. 2010 Drag reduction of a 3D bluff body using coherent streamwise streaks. *Exp. Fluids* **49** (5), 1085–1094.

PUJALS, G., GARCÍA-VILLALBA, M., COSSU, C. & DEPARDON, S. 2009 A note on optimal transient growth in turbulent channel flows. *Phys. Fluids* **21**, 015109.

REDDY, S. C., SCHMID, P. J., BAGGETT, J. S. & HENNINGSON, D. S. 1998 On the stability of streamwise streaks and transition thresholds in plane channel flows. *J. Fluid Mech.* **365**, 269–303.

SCHMID, P. J. & HENNINGSON, D. S. 2001 *Stability and Transition in Shear Flows*. Springer.

TANNER, M. 1972 A method for reducing the base drag of wings with blunt trailing edges. *Aeronaut. Q.* **23**, 15–23.

ZDRAVKOVICH, M. M. 1981 Review and classification of various aerodynamic and hydrodynamic means for suppressing vortex shedding. *J. Wind Engng Ind. Aerodyn.* **7**, 145–189.